Scanning Microscopy

Volume 9 | Number 2 Article 2

6-5-1995

From Scattering and Recoiling Spectrometry to Scattering and Recoiling Imaging

M. M. Sung
University of Houston

V. Bykov
University of Houston

A. Al-Bayati
University of Houston

C. Kim
University of Houston

S. S. Todorov
University of Houston

See next page for additional authors

From Scattering and Recoiling Spectrometry to Scattering and Recoiling Imaging

Authors
M. M. Sung, V. Bykov, A. Al-Bayati, C. Kim, S. S. Todorov, and J. W. Rabalais

Scanning Microscopy, Vol. 9, No. 2, 1995 (Pages 321-330) 0891-7035/95$5.00+.25
Scanning Microscopy International, Chicago (AMF O'Hare), IL 60666 USA

FROM SCATTERING AND RECOILING SPECTROMETRY TO SCATTERING AND RECOILING IMAGING

M. M. Sung, V. Bykov, A. Al-Bayati, C. Kim, S. S. Todorov and J. W. Rabalais*

Department of Chemistry, University of Houston, Houston, Texas 77204-5641

(Received for publication March 7, 1995 and in revised form June 5, 1995)

Abstract

A new ion scattering technique, called scattering and recoiling imaging spectrometry (**SARIS**), is being developed. The SARIS technique uses a large, position sensitive microchannel plate (MCP) and time-of-flight methods to capture images of scattered and recoiled particles from a pulsed keV ion beam. These images combine the advantage of atomic scale microscopy and spatial averaging simultaneously since they are created from a macroscopic surface area but they are directly related to the atomic arrangement of the surface. This paper describes the basis of the SARIS technique, the instrument which is under development, and the scattering and recoiling imaging code (**SARIC**) for simulation of the classical ion trajectories. Time-of-flight scattering and recoiling spectrometry (TOF-SARS) data are used to emulate the SARIS images for the case of 4 keV Ne^+ scattering from a Pt{111} surface. The observed scattering intensity patterns are characterized by their complex and rich structure. These experimental images are simulated by use of the SARIC program. The abundance of information contained in the images can be used to identify the type of surface being studied and its structure. The extraction of numerical values for the interatomic spacings, relaxations, reconstructions, and adsorbate site positions is accomplished by comparing the experimental and simulated images. Quantitative comparisons are made through the use of a reliability, or R, factor, which is based on the differences between the two images. The SARIS development will move low energy ion scattering into the realm of surface imaging techniques.

Key Words: Ion scattering, ion recoiling, surface imaging, surface structure, surface elemental analysis, position-sensitive detection, classical ion trajectory simulations.

*Address for correspondence:
J. Wayne Rabalais, address as above.
Phone no.: (713) 743-3282 / FAX no.: (713) 743-2709
E-mail: RABALAIS@JETSON.UH.EDU

Introduction

Low energy ion scattering spectrometry (ISS) had its beginning as a modern surface analysis technique in 1967 [11] when the possibility of both elemental and structural analyses was first demonstrated. During the 1970's, it was clearly shown [5, 6, 7] that direct structural information could be obtained from ISS. Interest in ISS as a surface structure technique grew rapidly during the 1980's, primarily due to advances such as coaxial ($\approx 180°$) backscattering [1, 2] for simplification of the interpretations and the use of time-of-flight techniques [9] in scattering and recoiling for efficient detection of both ions and fast neutrals. Research in our own laboratory over the past eleven years has developed an ISS technique called time-of-flight scattering and recoiling spectrometry (TOF-SARS) [4]. This work has demonstrated the use of TOF-SARS for surface elemental analysis and for determining surface periodicity, structure, and interatomic spacings to an accuracy of < 0.1 Å.

Through these advances in ISS and related techniques such as field ion microscopy (FIM), scanning tunneling microscopy (STM), and atomic force microscopy (AFM), **it is now realized that a surface structural technique is needed that can produce element-specific atomic structure information on a time scale of less than 1 second.** As a move in this direction, we are developing a technique called scattering and recoiling imaging spectrometry (**SARIS**) which has resulted from our TOF-SARS experience. The purpose of this paper is to present a preliminary report on the SARIS project. The paper is organized as follows. The next section provides a brief description of the TOF-SARS technique, the type of data obtained, and the limitations. In the third section, the SARIS technique and classical ion trajectory simulations used in interpreting SARIS data are described. Preliminary data on a Pt{111} surface, acquired by using TOF-SARS to emulate SARIS, is presented and interpreted in the fourth section. Pt{111} was chosen as a model surface for this demonstration because it does not reconstruct and it provides a stable well-ordered surface. The advantages of SARIS are exposed in the conclusions section.

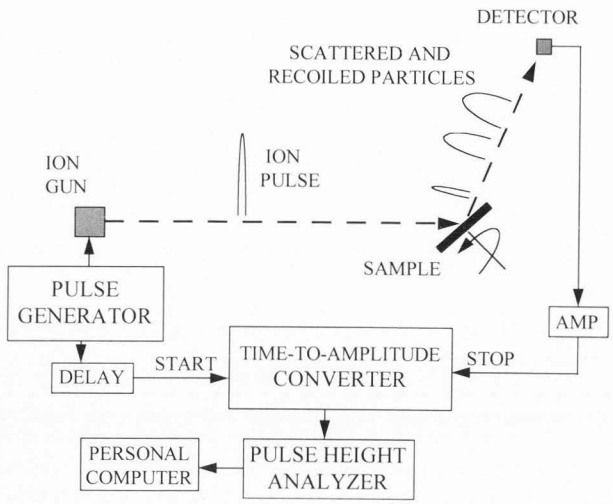

Figure 1. Schematic diagram of a time-of-flight scattering and recoiling spectrometer (TOF-SARS).

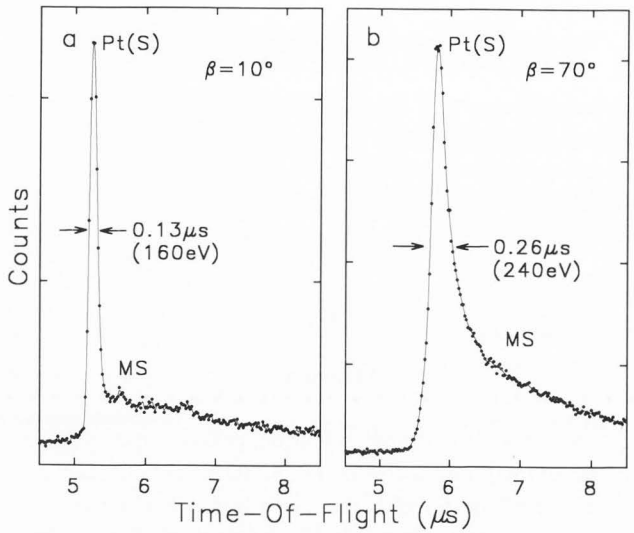

Figure 2. TOF-SARS spectra of 4 keV Ne^+ scattering from a clean Pt{111} surface using a normal beam incident angle (α = 90°) and scattering (exit) angles of **(a)** β = 100° (θ = 10°) and **(b)** θ = 160° (β = 70°). Single and multiple scattering features are denoted by S and MS, respectively. A schematic of the coordinate system used is shown later in Figure 6.

Time-Of-Flight Scattering and Recoiling Spectrometry (TOF-SARS)

In the TOF-SARS technique [4], a pulsed 1-5 keV noble gas ion beam scatters and recoils particles from a solid surface. These scattered and recoiled particles are velocity analyzed by time-of-flight techniques and detected directly by channel electron multipliers which collect particles leaving the surface in small solid angles, ca. 10^{-4} sr. These detectors are sensitive to both ions and fast neutral atoms, i.e., atoms with kinetic energies greater than about ca. 800 eV. A simplified schematic diagram illustrating the technique is shown in Figure 1. As a result of this energy discrimination by the detector and the μs time scale used, the TOF spectra contain only fast atomic species that result from quasi-binary collisions as shown in Figure 2. The kinematics of such processes can be calculated from classical mechanics, and classical ion trajectory calculations can be used to simulate the TOF spectra. Slow secondary ions, as observed in secondary ion mass spectrometry (SIMS), are not detected in TOF-SARS. Elemental analyses are achieved by converting the velocity distributions into energy distributions and relating these to the masses of the target atoms through the kinematic relationships that describe classical scattering and recoiling. Structural analyses are achieved by monitoring the scattered and recoiled particle intensities as a function of both beam incident angle α to the surface and crystal azimuthal angle δ. The anisotropic features in these α- and δ-scans are interpreted by means of shadow cone analysis data set; this is typically on the order of several hours. The reason for this is that individual data points in incident angle α and azimuthal angle δ space must be collected by stepping through the α and δ angles in intervals of 2° or less and collecting TOF spectra at each step. Since this procedure is time consuming, it is necessary to stop at regular intervals and refurbish the surface, i.e., clean to expel adsorbed residual gases, readsorb desired gases, or reanneal to achieve a well-ordered surface. The data acquisition time could be shortened by detecting the scattered and recoiled particles simultaneously using a detector which collects a large solid angle while the sample remains stationary.

Scattering and Recoiling Imaging Spectrometry (SARIS)

Experimental technique

In the SARIS technique, a large area, position sensitive, microchannel plate (MCP) is used to capture a large solid angle of the scattered and recoiled particle flux. This method records both in- and out-of-plane scattering and recoiling while eliminating the need for stepping through incident and azimuthal angles, thereby greatly decreasing the data acquisition time. Two research groups have previously developed [8, 12, 14] related large solid angle instruments. These experiments were successful in that they demonstrated that valuable structural information could be obtained, however the images represented convoluted processes and suffered

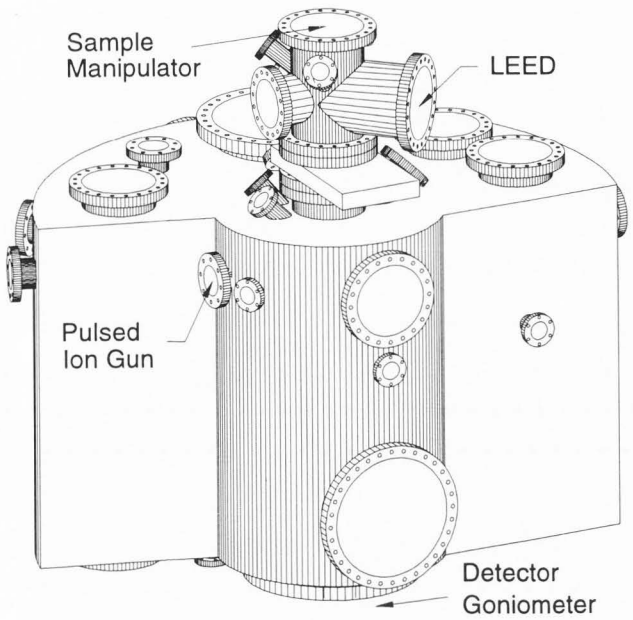

Figure 3. Schematic drawing of the new chamber for scattering and recoiling imaging spectroscopy (SARIS).

from high backgrounds due to the lack of mass and energy selection resulting from the lack of gating capabilities. The SARIS instrument uses TOF analysis and selective gating. This method collects both the ejected ions and fast neutrals and disperses scattered and recoiled particles according to their velocities as a function of the projectile/target atom masses and the deflection angle θ. This eliminates the problems and limitations of the previous instruments.

Details of the SARIS instrument are as follows. The ultra-high vacuum chamber is in the shape of a large half-cylinder {radius 24 inches (61 cm) and height 29 inches (73.7 cm)} with a wedge cut out of one side for the ion beam, as shown in Figure 3. A pulsed 1-5 keV noble gas ion beam impinges on the sample from a port in this wedge. A precision sample manipulator, mounted on a small vacuum chamber placed above the top center flange, is used to introduce samples into the measurement position. The MCP detector is mounted on a goniometer through the bottom center flange, allowing horizontal and vertical movement as well as translation away from the sample in order to change the solid angle of collection and flight length.

A schematic of the detector and associated electronics is shown in Figure 4. A rectangular (75 x 95 mm) chevron type MCP is used for detection of scattered and recoiled particles. A resistive anode encoder (RAE) plate of shape identical to the MCP is mounted behind the MCP. Each scattered and recoiled particle that strikes the MCP generates an electron charge which dissipates in the RAE. The four signals generated at each corner of the RAE are picked up by a set of capacitors, A, B, C and D, and are transmitted inside the chamber along 50 ohm coaxial cables. These signals are amplified by a set of preamplifiers mounted on the scattering chamber. The amplitude of these signals depends on the position (X and Y) at which the electron charge from the MCP strikes the RAE, i.e., the position of the particle hitting the MCP.

The determination of the position (X and Y) and the time-of-flight (TOF) information of each particle striking the MCP represents the basis of the SARIS instrument. The X and Y data are calculated by an analog computer using the A to D signals and the following formulae: $X = (A + B) / (A + B + C + D)$ and $Y = (B + C) / (A + B + C + D)$. The X and Y analog signals are converted into digital format using flash type analog to digital converters. The number of bits is 6 for each X and Y datum, giving a spatial resolution of 1.1 and 1.4 mm for the X and Y axis, respectively. A set of logic circuits, mounted in the preamplifier box, control the validity of events detected. If the amplitude of the summing signal (A + B + C + D) falls outside a certain range or the time difference between successive events is too small, the events are neglected. The pre-amplifier and control logic circuits have a dead time of $\cong$300 ns, giving a maximum data rate of 1 to 2 M counts/sec.

The TOF data are measured using a multiple-hit time-to-digital converter (TDC). This is described as follows: The START signal is received from a pulse generator (used for pulsing the primary ion beam) after some delay (typically a few μs), which accounts for the TOF of particles from the pulsing plates in the ion beam line to the sample. When a valid event is detected, a stop signal, generated by the logic circuits, is sent to the TDC. The STOP signal is the same signal used for converting the X-Y data to digital format (indicated by the CONVERT signal in Fig. 4). The TDC consists of 2 synchronous 4-bit binary counters connected in series to give 8-bit time information; the TDC runs off a 60 MHz transistor-transistor-logic (TTL) oscillator. The STOP signal transfers the time information from the counter to a temporary register; it does not stop the counter, i.e., it leaves the counter ready to determine the TOF of the following events. The system is designed to have a time resolution of 50 ns.

A certain time after generating the stop signal, the control logic circuits generate a strobe signal of width 200 ns to transfer the X, Y and TOF data to a FIFO (first-in-first-out) buffer memory. The buffer size is 16 words and each word is 20 bits wide, divided as follows: first 6 bits, X data; second 6 bits, Y data; and last 8 bits, TOF data. These data are continuously transferred to a histogramming buffer memory of 1 M (2^{20} = 1 M memory address) words and each word is 16 bits

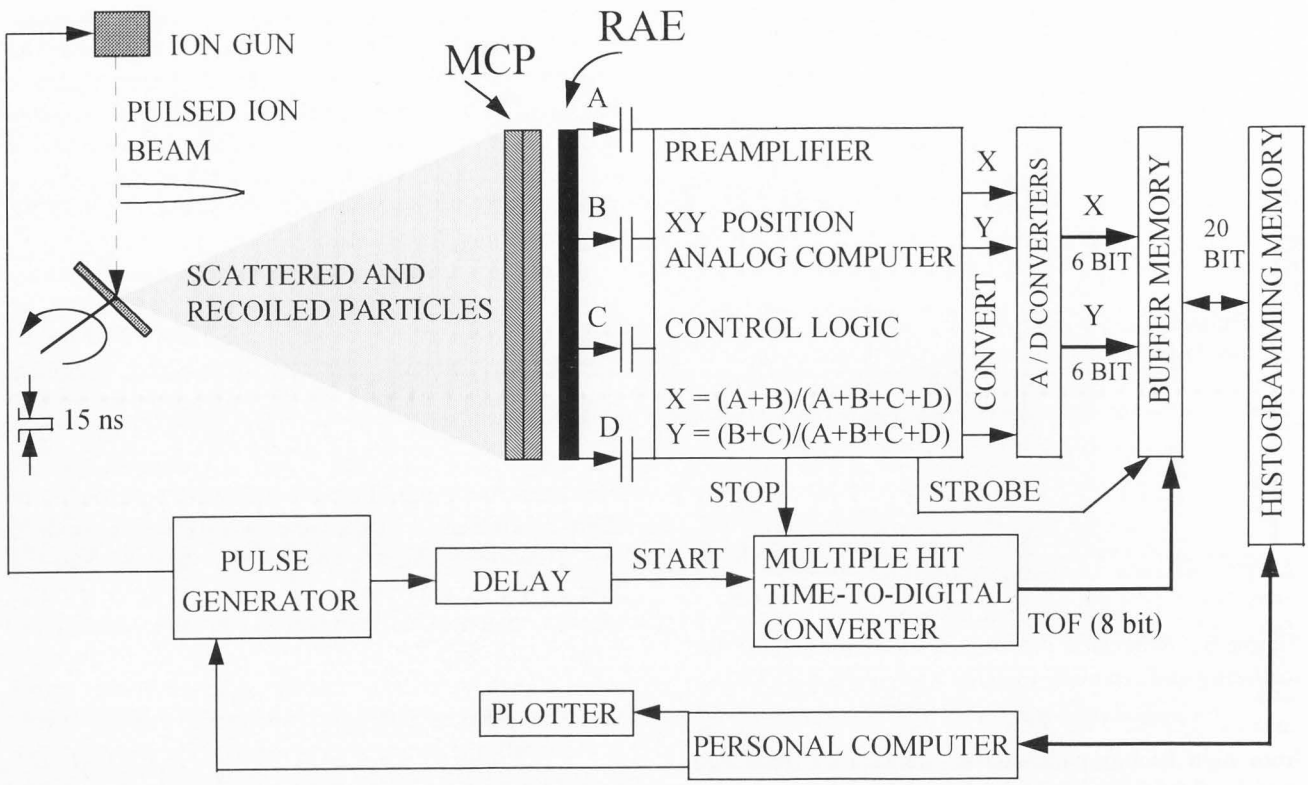

Figure 4. Schematic drawing of the detection system for SARIS. MCP = position sensitive microchannel plate; RAE = resistive anode encoder.

---

wide, allowing a maximum accumulation of 64K counts for each specific X, Y and TOF combination. The data in the histogramming memory can be transferred to a host computer at the end of or during data accumulation. Although the latter mode allows "real time" monitoring of the data, it increases the time of data acquisition. A typical acquisition time for one image using the first mode is expected to be 15 minutes, which is at least a factor of 10 faster than the current TOF-SARS system.

Elemental analyses. Elemental analyses of surfaces will be obtained by measuring the flight times of ions and atoms scattered and recoiled from the sample to specific bins of pixels on the MCP's using standard TOF-SARS timing methods.

Surface structural determinations. Surface structural determinations will be obtained by analyzing the shadowing and blocking features in the images, both qualitatively and quantitatively, through the application of three-dimensional classical trajectory calculations.

Simulation method

The intensity patterns of the scattered ions and recoiled atoms detected by the large-area MCP detector are characterized by their complex and rich structure. This abundance of information provides a convenient way to identify the type of surface being analyzed but makes the quantitative interpretation more difficult. The extraction of numerical values for the interatomic spacings, relaxations and reconstructions of the surface necessitate a similarly complex interpretative apparatus. This has led to the development in our laboratory of a computer simulation code tailored specifically to modeling the scattering and recoiling of keV ions from crystal surfaces. This scattering and recoiling imaging code (**SARIC**) is based on the binary collision approximation (BCA), i.e., it models the trajectories of the energetic particles as a series of straight lines corresponding to the asymptotes of the scattering trajectories due to sequential binary collisions. For the keV range of energies discussed here, the BCA has been shown to be valid [3].

In the SARIC program, the points of impact of the primary ions are distributed randomly over a bombardment segment which is chosen in accordance with the surface symmetry. Ions are generated until satisfactory statistics are accumulated, usually of the order of 5×10^6 primaries. The Ziegler, Biersack and Littmark (ZBL) universal potential [15] is used to describe the screened Coulomb interaction between the atoms. Inelastic energy losses constitute only a minor fraction of

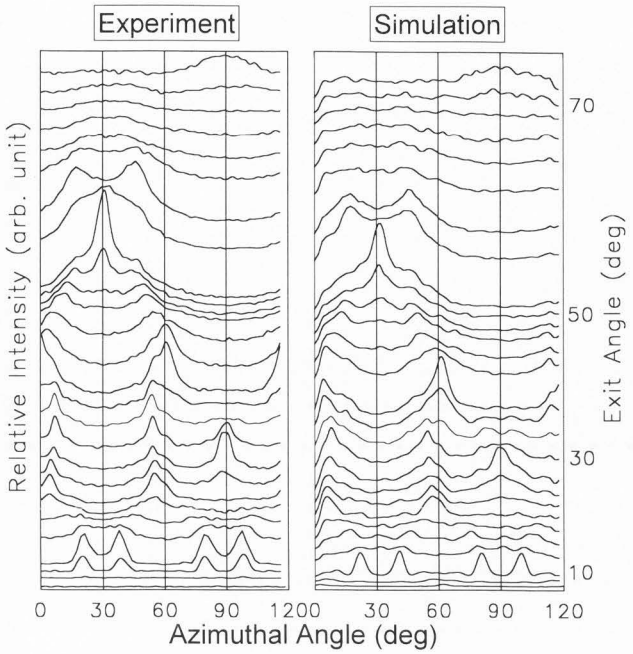

Figure 5 (left). Experimental TOF-SARS scans of 4 keV Ne^+ scattering intensity from a clean Pt{111} surface at constant exit angles β as a function of azimuthal angle δ. **Figure 5 (right).** SARIC simulations of the TOF-SARS data.

---

the scattered and recoiled energies and are consequently neglected. The primary ion moves undeflected for a distance d determined by the ion-target atom combination. A search for collision partners is then performed within a target cylinder of length d perpendicular to the ion's direction of motion and radius equal to the maximum impact parameter. The scattering angle is determined and the new velocities of the scattered ion and recoiled atom are calculated. Since primary ions and recoils which have undergone more than a few collisions do not contribute to the detected peak intensities, an ion which after several collisions does not have an outward directed momentum component is dropped from consideration and a new primary ion is generated and followed.

In the case when more than one collision partner is found in the search volume, the program models quasi-simultaneous interactions in the following manner. The recoil angle and energy are calculated for each collision partner. The energy and momentum of the scattered and recoiled particles are then obtained from conservation laws. This allows treatment of focusing effects when an energetic ion or atom passes through, e.g., a ring of crystal atoms. Simulation of such events using the sequential BCA approach would produce incorrect results.

Additional measures have been taken to speed up the calculation so that it may be performed on a personal

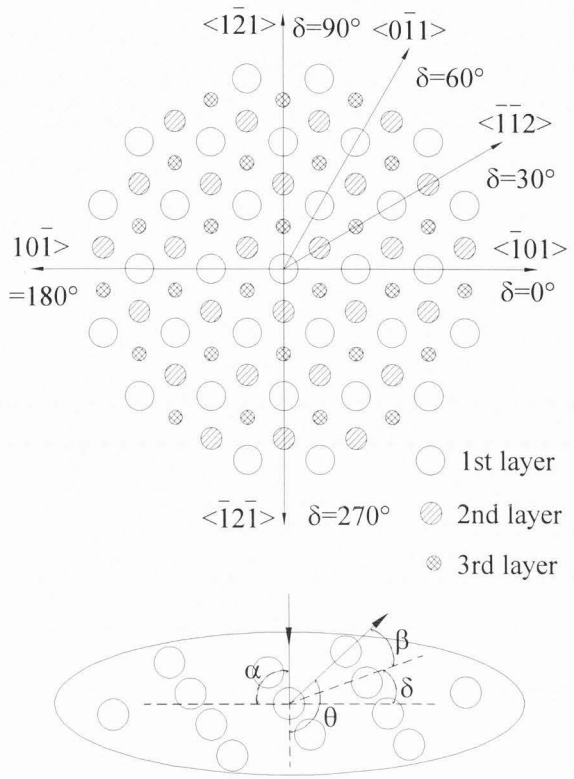

Figure 6. Schematic drawing of the Pt{111} surface along with the definition of the azimuthal angles δ.

---

computer. The deflection angles, θ, in the center-of-mass system are precalculated as a function of reduced ion energy and reduced impact parameter. A relatively small target is described, 100-150 atoms arranged in 3-5 layers, which is sufficient for reliable simulation of the scattering events since they are essentially short-range phenomena.

The crystalline target is described using initial "guesses" about the positions of the target atoms; these usually correspond to the unreconstructed surface. After a sufficient number of detected events have been simulated, the computed and experimental intensity profiles are compared. A reliability, or R, factor is calculated based on the differences between these profiles [13]. The positions of the target atoms are then adjusted to produce successively lower values of the R factor, i.e., better fits to the experiment. In the case of simple surfaces, this is a straightforward minimization as a function of varying lattice parameter. In the case of more complex surfaces, this procedure also includes relaxation and reconstruction.

TOF-SARS Emulation of SARIS Results

TOF-SARS can be used to emulate SARIS results

Experimental Results

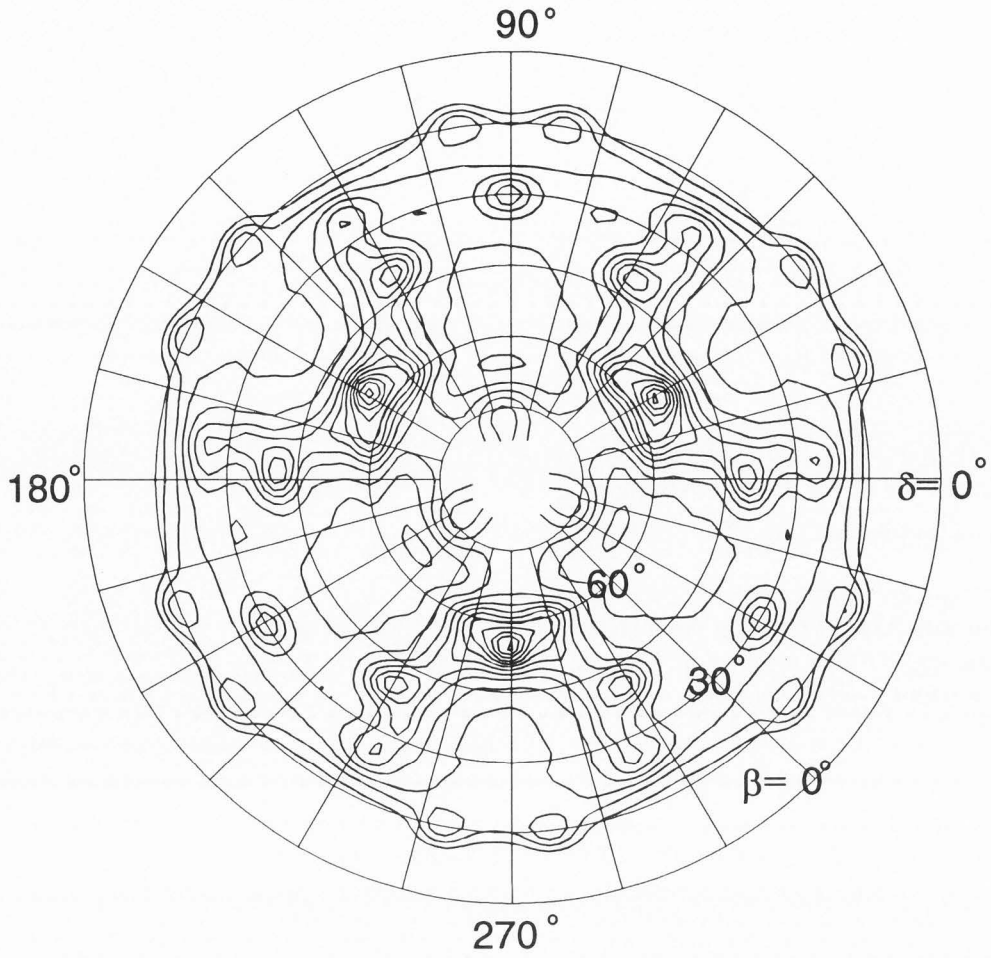

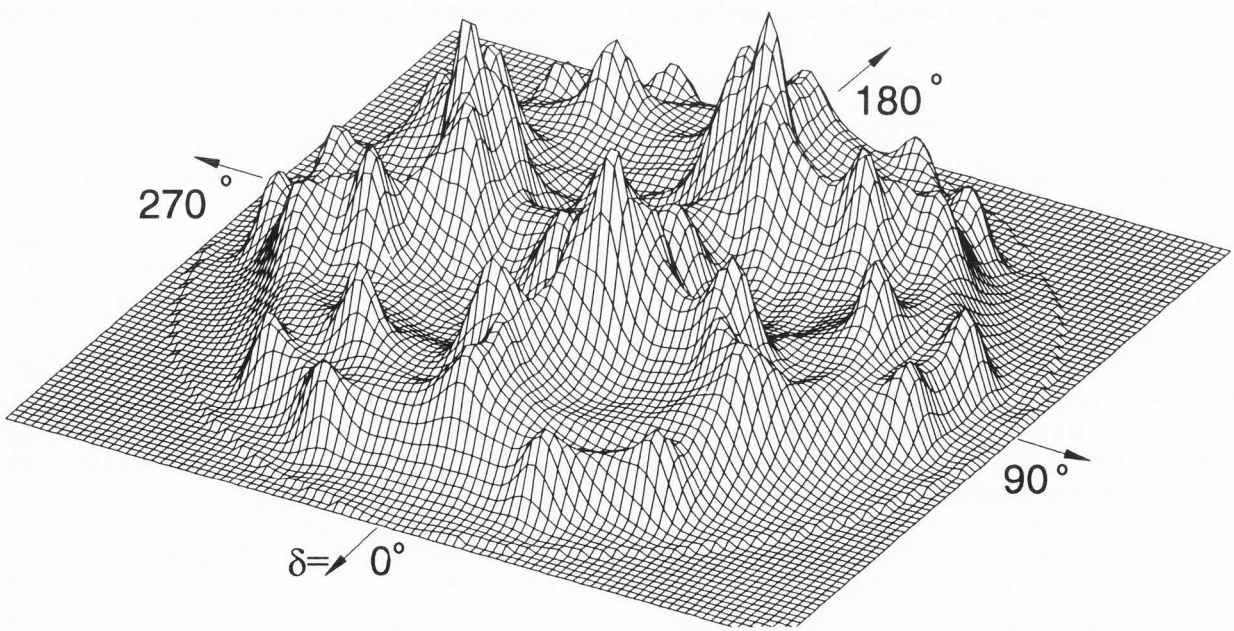

Figure 7 (on the facing page). TOF-SARS emulation of the SARIS images shown as a contour and a three-dimensional plot.

---

by the following method. TOF-SARS spectra are collected with the beam incident along the surface normal and the detector fixed at a specific scattering (or exit) angle, while the surface is rotated about its normal (azimuthal angle rotation). This provides azimuthal angle δ scans at fixed particle exit angle β. Such scans of scattering intensity versus azimuthal angle are shown parametrically for a series of exit angles for 4 keV Ne^+ scattering from a clean Pt{111} surface in Figure 5. The scattering intensities were determined by integrating a window of $\Delta t = 0.11\ \mu s$ ($\Delta E = 150$ eV) centered about the maximum of the scattering peak. Simulations of this data using the SARIC program are shown on the right side of the figure. The azimuthal angles are defined as shown in Figure 6, i.e., $0° = <\bar{1}01>$, $30° = <\bar{1}\bar{1}2>$, $60° = <0\bar{1}1>$, and $90° = <1\bar{2}1>$. The collection time for the data in Figure 5 is about 15 hours; using SARIS, this acquisition time is expected to be reduced by at least a factor of 30. Also, SARIS will provide higher resolution due to the small pixel sizes on the detector and higher accuracy since it is not necessary to rotate the sample in order to collect data.

The data of Figure 5 can be plotted in a manner to represent the type of images that will be collected by SARIS. Consider the intensities of scattered ions detected by a hemispherical detector positioned such that the target is at the center of the hemisphere and the ions are incident normal to the target surface along the axis of symmetry/revolution which we define as the Z-axis. Each point on such a detector is described by two angles, the azimuthal angle δ, defined as the angle of rotation about the Z-axis, and the exit angle β, defined as the angle above the plane of the target. Figure 7 shows the projection of this detector onto the plane of the target, i.e., the radial distance from the center corresponds to the exit angle β and the distance along the circumference of the circle corresponds to the azimuthal angle δ. Note that the experimental data was actually collected for only the azimuthal range $\delta = 0°$-$135°$; the symmetrical images of Figure 7 were constructed by translating this data to the other symmetrical azimuthal positions. Experimental data were not collected for exit angles within 17.5° from the normal due to instrumental limitations. Scattered atom intensities can be represented as either contours or three-dimensional structures. These images exhibit a rich and complicated structure. The three-fold symmetry of the {111} surface is clearly revealed in the contour plot.

The SARIC simulations of Figure 5 were also plotted in the above manner as shown in Figure 8. There is

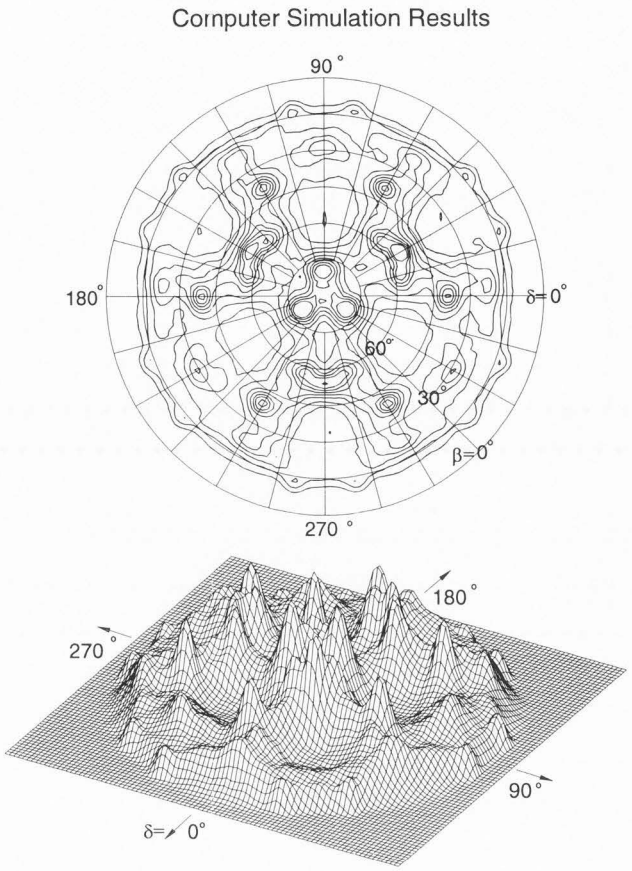

Figure 8. SARIC simulation of the images in Fig. 7.

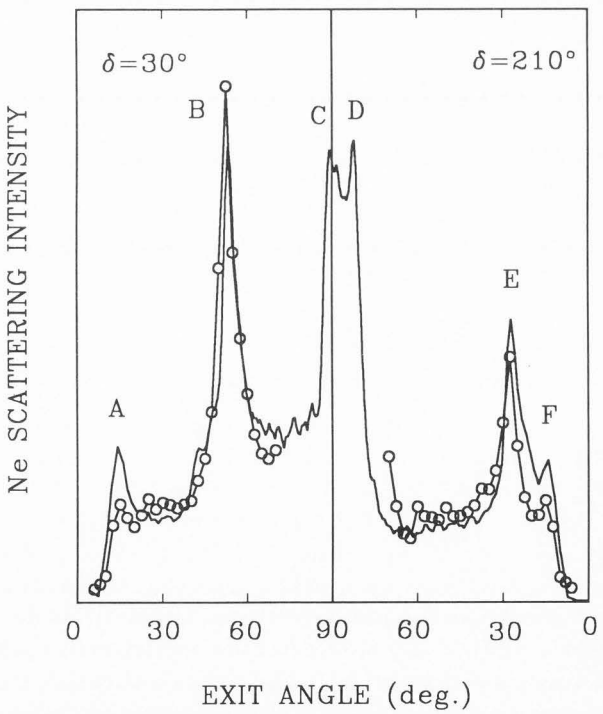

Figure 9. Cut through the data of Figs. 7 and 8 along the azimuths $\delta = 30°$ and 210°.

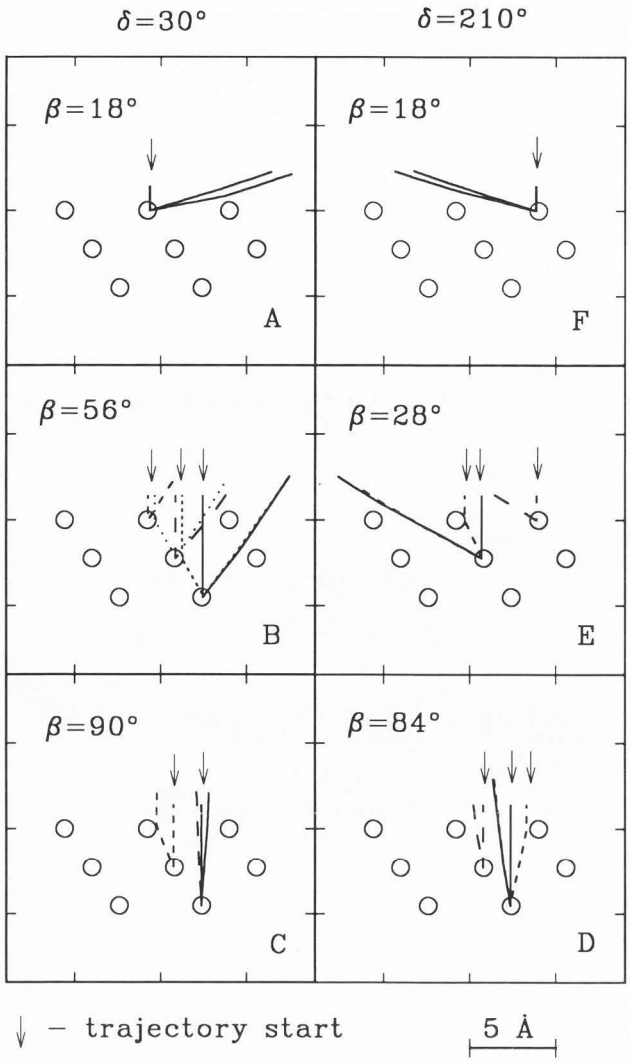

Figure 10. Trajectory simulations of the scattering events responsible for producing the peaks observed in Figure 9. The peaks are identified by the letters within each box. Solid, dashed, and dotted lines are used to illustrate processes of decreasing importance.

---

good qualitative agreement between the experimental and simulated images. In order to obtain a more quantitative comparison and a description of the microscopic processes contributing to these images, cuts through the data of Figures 7 and 8 were made along the $\delta = 30°$ $<\bar{1}\,1\,2>$ azimuth and the $\delta = 210°$ $<11\bar{2}>$ azimuth, as shown in Figure 9. The experimental data are shown as points and the simulation is shown as a line. The calculated results were obtained using a planar version of SARIC which does not take into account out-of-plane events and focusing by rings of surface atoms. This causes the central peak C at $\beta = 90°$ to be somewhat lower than in the results of the full three-dimensional simulation shown in Figure 8. The planar scattering mechanisms are responsible for the sharp peaks observed, the exception being part of the central peak, labeled C. The scattering trajectories which make the dominant contributions to the detected peaks of Figure 9 are identified in Figure 10.

We now discuss the detailed scattering mechanisms which produce each of the peaks in Figure 9. Peaks A and F at $\beta = 18°$, are due entirely to a single mechanism, namely the blocking of ions scattered from a 1st-layer atom by the neighboring 1st-layer atom to the right or left. Peak B at $\beta = 56°$ is due to a number of trajectories, of which $\sim 1/2$ are due to focusing of atoms scattered by a 3rd-layer atom by the lens formed by the adjacent 2nd- and 1st-layer atoms. The focusing of incoming ions onto the lower layer by the shadow cone of atoms in the 1st- or 2nd-layer contributes to $\sim 10\%$ of the trajectories. Ions which scatter from the 2nd-layer and are focused on their outward trajectory by the blocking cones of the 1st-layer atoms contribute to $\sim 1/3$ of the trajectories. Peak E at $\beta = 28°$ consists almost exclusively of two contributions: $\sim 2/3$ is due to focusing of incident atoms by the shadow cone of a 1st-layer atom onto a 2nd-layer atom from which they are then scattered. The remainder is due to simple scattering from 1st-layer atoms. Peak C at $\beta = 90°$ is due to atoms scattered from the 2nd- and 3rd-layer followed by focusing from 1st-layer atoms and, in the case of 3rd-layer scattering, focusing from 2nd-layer atoms also. The relative contributions of these processes are $\sim 1/3$ for 2nd-layer scattering, $\sim 1/3$ for 3rd-layer scattering with 2nd-layer focusing, and $\sim 15\%$ for 3rd-layer scattering with 1st-layer focusing. Peak D at $\beta = 84°$ is due to blocking and focusing of atoms scattered from the 2nd-layer by 1st-layer atoms ($\approx 10\%$), blocking of atoms scattered from the 3rd-layer by 2nd-layer atoms ($\sim 1/3$), and the remainder to a number of mechanisms, the most important among which are out-of-plane versions of the above two types of events.

The above analysis of the individual trajectories in Figure 10 shows that the peaks observed in the SARIS images result from scattering and blocking events which involve the 1st- through 3rd-atomic layers of the crystal surface. As a result, the positions and orientations of the SARIS peaks are sensitive to both lateral and vertical interatomic spacings. Through this sensitivity, direct information on surface periodicity, reconstruction, relaxation, and adsorbate site positions can be obtained. Since these trajectories are not simple, three-dimensional trajectory simulations are required to obtain a detailed interpretation of the images.

The data presented in this paper were all collected under the conditions of maximum sampling depth, i.e., with the incident beam directed along the surface normal SARIS images collected with the beam directed along

low incident angles will typically sample only the 1st- and 2nd-atomic layers and will also contain recoil data. The recoil data are particularly important for studying light atoms such as hydrogen, carbon, and oxygen.

Conclusions

The new technique of scattering and recoiling imaging spectrometry (SARIS) is under development at the University of Houston. TOF-SARS emulation of SARIS images shows that the images are rich in structural detail from which the surface symmetry can be directly observed and structure determinations can be made. SARIS will have direct application for monitoring dynamic processes at surfaces, such as thin film growth, surface diffusion and atomic migration, reconstruction, chemisorption and surface reactions, surface damage, etc. on a time scale of several minutes.

The primary advantages of SARIS are as follows: (**1**) element specific, (**2**) sensitive to all elements, including hydrogen, (**3**) directly exposes the surface symmetry, (**4**) "real space" analysis, (**5**) applicable to any surface, (**6**) measures interatomic spacings to < 0.1 Å in favorable cases, (**7**) one monolayer or subsurface sensitivity available, and (**8**) fast enough to monitor dynamic processes on a time scale of minutes.

Acknowledgment

This material is based on work supported by the National Science Foundation under Grant No. CHE-9321899.

References

[1] Aono M, Hou Y, Souda R, Oshima C, Otani S, Ishizawa Y, Matsuda K, Shimizu R (1982a). Interaction potential between He^+ and Ti in a keV Range as revealed by a specialized technique in ion scattering spectroscopy. Jpn. J. Appl. Phys. **21**: L670-L672.

[2] Aono M, Hou Y, Oshima C, Ishizawa Y (1982b). Low-Energy Ion Scattering from the Si(001) Surface. Phys. Rev. Lett. **49**: 567-570.

[3] Eckstein W, Hou M (1988). Angular ejection distributions in low energy single crystal sputtering: The relation to the interatomic potential. Nucl. Instrum. Meth. Phys. Res. **B31**: 386-392.

[4] Grizzi O, Shi M, Bu H, Rabalais JW (1990). Time-of-flight scattering and recoiling spectrometer (TOF-SARS) for surface analysis. Rev. Sci. Instrum. **61**: 740-752.

[5] Heiland W, Taglauer E (1977). The backscattering of low energy ions and surface structure. Surf. Sci. **68**: 96-107.

[6] Heiland W, Iberl F, Taglauer E, Menzel D (1975). Oxygen adsorption on (110) silver. Surf. Sci. **53**: 383-392.

[7] MacDonald RJ, Heiland W, Taglauer E (1978). A comparison of surface analysis using ion scattering, ion-produced photons, and secondary ion emission. Appl. Phys. Lett. **33**: 576-578.

[8] Niehof A, Heiland W (1990). Experimental realisation of low-energy surface channeling. Nucl. Instrum. Meth. B **48**: 306-310.

[9] Rabalais JW (1990). Scattering and recoiling spectrometry: An ion's eye view of surface structure. Science **250**: 521-527.

[10] Shi M, Grizzi O, Bu H, Rabalais JW, Rye RR, Nordlander P (1989). Time-of-flight scattering and recoiling spectrometry. III. The structure of hydrogen on the W(211) surface. Phys. Rev. B **40**: 10163-10180.

[11] Smith DP (1967). Scattering of low-energy noble gas ions from metal surfaces. J. Appl. Phys. **38**: 340-347.

[12] Williams RS, Yarmoff JA (1983). Surface structure analysis from low-energy ion backscattering angular distributions. Nucl. Instrum. Meth. **218**: 235-240.

[13] Xu ML, Tong SY (1985). Multilayer relaxation for the clean Ni(110) surface. Phys. Rev. **31**: 6332-6336.

[14] Yarmoff JW, Blumenthal R, Williams RS (1986). Low energy ion backscattering angular distributions of $^6Li^+$ from Cu(001). Surf. Sci. **165**: 1-20.

[15] Ziegler JF, Biersack JP, Littmark U (1985). The Stopping and Range of Ions in Solids. Ziegler JF (ed.). Pergamon Press, New York. pp. 32-48.

Discussion with Reviewers

D.D. Koleske: As demonstrated in the paper, oriented single crystal surfaces or surfaces with ordered adsorbates can be studied with this technique. To what extent could the SARIS technique be applied to partially disordered surfaces or surfaces with no periodic structure, but chemically phase separated domains?

Authors: Disorder appears in the SARIS images as broadening of the sharp scattering and recoiling focusing features observed in well-ordered surfaces. The degree of disorder can be quantitatively assessed by comparison of the image from a disordered surface with that from a well-ordered surface.

D.D. Koleske: What is the elemental sensitivity to the 2nd and deeper layers? Could the angle the beam makes with the surface, i.e. α, be varied to selectively enhance signal from the 2nd and deeper layers? Such a capability might prove useful in studying III-V semiconductors

or layered binary alloys.

Authors: Sensitivity to subsurface layers is directly dependent on the beam incident angle α as shown in one of our previous publications [Surface Sci. **296**, 213 (1993)]. Grazing incidence α results in first-layer sensitivity while high α values probe subsurface layers. The data reported here uses normal incidence, hence the sensitivity to the first- through third-layers. This feature is indeed very useful for probing layered materials, as our recent work [Surface Sci. **322**, 116 (1995)] on the III-IV semiconductors InP, GaAs, and InAs shows.

D.D. Kleske: What is the relative fraction of ions to neutrals and could the ions be selectively discriminated from the neutral signal?

Authors: The scattered and recoiled ion fractions are typically $< 10\%$ and $< 5\%$, respectively. The ions can be separated from the neutrals by electrostatic deflection, as we have previously shown [Phys. Rev. Lett. **69**, 188 (1992)]. Since the ion fractions are a sensitive function of surface work function, surface cleanliness, beam incident and azimuthal angles, etc., it is necessary to collect both the ions plus neutrals in order to obtain data which are dependent only on changes in structural features and not neutralization phenomena.

D.C. Jacobs: What is the solid angle of collection in the current SARIS geometry? Will the angle of the imaging detector or the angle of the surface require any scanning during data acquisition in order to cover a solid angle larger than that associated with the detector?

Authors: The solid angle of collection depends on the distance between the detector and the sample. Since we can vary this distance from 10 to 54 cm, the rectangular solid angle defined by the detector varies from 41.1° x 50.8° to 8.0° x 10.2°. At 10 cm, the solid angle is large enough to reveal the symmetry of the surface and the angles of specific focusing features, albeit with poor spatial and temporal resolution. Retracting the detector along a direction corresponding to one of the focusing features amounts to "zooming-in" on this feature, i.e., both the spatial and temporal resolution are improved. This ability to zoom-in allows detailed study of structural features.

D.C. Jacobs: What improvements would be required to further reduce the data acquisition time of SARIS from the estimated 15 minutes?

Authors: Faster position-sensitive read-outs are necessary in order to reduce the data acquisition time. The limit of the current resistive anode encoder is a dead time of ~ 300 ns, giving a maximum data rate of 1 to 2 M cts/s. New developments in read-outs, such as delay-line anodes, hold promise for faster data acquisition rates.

D.C. Jacobs: What incident ion currents and pulse widths are required by SARIS?

Authors: SARIS requires ion currents and pulse widths that are similar to TOF-SARS, i.e., ~ 1 nA/cm^2 and ~ 30 ns, respectively. Naturally, the sharper the pulse width, the sharper the spectrum; the planned pulse width for the SARIS is 10 ns.

D.C. Jacobs: How do TOF-SARS and SARIS compare in terms of the amount of surface damage inflicted by the incident ion beam during spectral acquisition?

Authors: Since the ion currents are the same, the amount of damage inflicted per unit time will be identical. However, since SARIS is able to collect an image in minutes and TOF-SARS requires hours, the former is far less damaging.

P.R. Watson: How sensitive is SARIS data (via simulation presumably as yet) to changes in surface geometry? Is the method more sensitive to changes parallel or normal to the surface?

Authors: SARIS has about the same sensitivity to surface geometry as does TOF-SARS, i.e., structural determinations are accurate to ~ 0.1 Å. The faster data acquisition time for TOF-SARS should allow monitoring of some surface dynamics, such as surface reconstruction, diffusion, disordering, melting, etc.

P.R. Watson: What is the likelihood of pushing the method to produce structure information on time scales of 1 second, as mentioned in the **Introduction**?

Authors: Faster data acquisition awaits improvements in the technology of position-sensitive detectors. We have confidence that acquisition times down to ~ 1 second will be feasible within the next few years.

P.R. Watson: Is there any possibility of inverting the data to avoid trial-and-error comparisons of theory and experiment?

Authors: This is an excellent question and one that we are currently working on. The answer is definitely "yes." It is possible to develop algorithms which use the features of the images to directly determine the structural model, hence avoiding the necessity for comparison between experiment and theoretical simulations.